RESEARCH PAPER

Wetland Mapping by Fusion of Airborne Laser Scanning and Multitemporal Multispectral Satellite Imagery

Maha Shadaydeh[a], András Zlinszky[b], Andrea Manno-Kovacs[a], and Tamas Sziranyi[a]

[a]Institute for Computer Science and Control of the Hungarian Academy of Sciences, Kende u. 13-17, H-1111 Budapest, Hungary; [b]Balaton Limnological Institute, Centre for Ecological Research of the Hungarian Academy of Sciences, Klebelsberg Kuno u. 3, H-8237 Tihany, Hungary

ABSTRACT
Wetlands play a major role in Europe's biodiversity. Despite their importance, wetlands are suffering from constant degradation and loss, therefore they require constant monitoring. This paper presents an automatic method for the mapping and monitoring of wetlands based on the fused processing of laser scans and multispectral satellite imagery, with validations and evaluations performed over an area of Lake Balaton in Hungary. Markov Random Field models have already been shown to successfully integrate various image properties in several remote sensing applications. In this paper we propose the Multi-Layer Fusion Markov Random Field (ML-FMRF) model for classifying wetland areas, built into an automatic classification process that combines multitemporal multispectral images with a wetland classification reference map derived from Airborne Laser Scanning (ALS) data acquired in an earlier year. Using an ALS-based wetland classification map that relied on a limited amount of ground truthing proved to improve the discrimination of land cover classes with similar spectral characteristics. Based on the produced classifications, we also present an unsupervised method to track temporal changes of wetland areas by comparing the class labellings of different time layers. During the evaluations, the classification model is validated against manually interpreted independent aerial orthoimages. The results show that the proposed fusion model performs better than solely image based processing, producing a non-supervised/semi-supervised wetland classification accuracy of 81-93% observed over different years.

1. Introduction

Despite their relatively small area, wetlands have an important contribution to Europe's biodiversity since they are crucial in regulating water flows, filtering water and carbon storage (Vymazal 2011), and preserving wildlife against intensive human presence. Although their importance is indisputable, wetlands are suffering from continuous degradation and loss (Reis et al. 2017; Davidson 2014). A major cause of wetland loss is the conversion to agricultural lands due to economic and population

---

CONTACT Andrea Manno-Kovacs. Email: andrea.manno-kovacs@sztaki.mta.hu

growth (Berry et al. 2016). Improper water management along with peat extraction and reed harvesting also put pressure on wetlands. To slow down the degradation and prevent the further loss of wetlands, several European and global multilateral agreements have been implemented, requiring regular monitoring of the extent and condition of wetlands.

This paper's main goal is to aid such monitoring tasks by presenting a methodology for automatic classification of wetland areas. Our study concentrates on the Lake Balaton area, which is a large (594 km^2 area) and shallow (3.3 m mean depth) lake in western Hungary. Half of the lake's shoreline is bordered by reed-dominated wetlands adding up to a total area of 11 km^2 (Zlinszky et al. 2012). The lake is under the protection of Natura 2000 and the Ramsar convention; both of them require regular spatial monitoring of wetland extent and condition. Such monitoring is currently performed through fieldwork, which can be extremely resource intensive. Earlier studies have drawn attention to the ongoing loss of wetland vegetation around Lake Balaton (Kovács et al. 1989). A time series of aerial images spanning the years 1951-2003 was analyzed in order to determine the cause of reed wetland die-back (Zlinszky 2013). Later on, an Airborne Laser Scanning (ALS) data was acquired in August 2010 around Lake Balaton in the framework of the EUFAR AIMWETLAB project by the NERC (Natural Environment Research Council) Airborne Research and Survey Facility (full technical details can be found in (Zlinszky et al. 2011)). The collected ALS data was successfully used for the categorization of wetland vegetation (Zlinszky et al. 2012).

Nowadays there are several functioning satellites that can provide high resolution remote sensing imagery for various applications, e.g., vegetation mapping and spatio-temporal change monitoring (Mui, He, and Weng 2015; Mandanici and Bitelli 2015; Benedek et al. 2015). Multispectral imagery (MS) acquires data from the visible, near infrared (NIR) and shortwave infrared (SWIR) range. These spectral bands can be efficiently used for vegetation monitoring through different spectral indices, such as the widely used Normalized Difference Vegetation Index (NDVI) (Weier and Herring 1999). However, for MS images with limited spectral bands, it may be difficult to distinguish the different vegetation classes having similar spectral characteristics. To compensate for this drawback, multi-seasonal data from different sensors can be exploited in the segmentation process. Selecting suitable features from this heterogeneous data to serve as inputs for a classification process can improve the classification's accuracy (Lu and Weng 2007).

Due to its ability to resolve vegetation structure and texture in high resolution, ALS is rapidly emerging as a sensor for vegetation mapping (Eitel et al. 2016) (Pfeifer et al. 2015). Several recent wetland vegetation analysis methods concentrate on the combined use of ALS and multispectral Earth observation. In most applications, the topographical information of the scene extracted from ALS data is used to increase the discrimination accuracy of land-cover classes having similar spectral characteristics (Alonzo, Bookhagen, and Roberts 2014). In (Rapinel, Hubert-Moy, and Clément 2015) multiseasonal, multispectral, high resolution (SPOT-5, Quickbird, KOMPSAT-2 and aerial) imagery is fused with ALS data to classify different vegetation patches present in wetlands; the aquatic vegetation of tropical wetlands in Northern Australia is analyzed in (Whiteside and Bartolo 2015) using Worldview-2 and ALS data to detect changes during and after the rehabilitation of a mining site. The method presented in (Niculescu et al. 2016) successfully discriminates different wetland vegetation classes in the Danube Delta applying ALS data, RADARSAT-2 and SPOT-5 satellite images.

However, due to its high cost, high-resolution ALS data collection is usually not repeated at regular time intervals (Eitel et al. 2016). On the other hand, satellite

sensors offer high temporal resolution and wide area coverage. Some of these satellite data are now freely accessible, but collecting the necessary large-scale ground reference data-sets through fieldwork is often prohibitively resource intensive. ALS data can allow for efficient and accurate up-scaling from field plots to landscape level (Levick, Hessenmöller, and Schulze 2016). Theoretically, if a satellite image is available close enough in time to the airborne campaign, the output of airborne data processing can be used as initial training data for categorizing the satellite imagery and the developed classifier can be transferred to different MS data collection dates preceding or succeeding the airborne data collection.

The main objective of this study is to demonstrate the above approach, developing a method for automatic classification of wetland areas that also enables the detection of the location as well as the type of change. The wetlands of the test area are situated among a challenging mosaic of land cover classes such as agricultural fields, urban areas, forests and grasslands. The extent of wetlands can vary very dynamically in time, depending on land use and hydrological conditions. The proposed method is developed based on the fusion of multitemporal MS imagery and ALS data. The fusion of multitemporal MS images of the same area aims to improve the identification of classes having rich seasonal spectral variations, such as wetlands. To further improve the discrimination of classes with similar spectral characteristics, we used the wetland classification map derived from ALS data in an earlier year in (Zlinszky et al. 2012) for initial training. In our current study, two MS images representing two different agricultural seasons (post- and pre-harvest) are selected to improve discrimination between agricultural vegetation and wetland class.

Remote sensing images often contain regions with similar local characteristics (intensity, colour, local statistics). Markov Random Field (MRF) models have the ability to quantify the spatial dependency among pixels by a mathematically well established methodology. MRF models were also shown to have excellent potential for the integrated analysis of spectral, semantic, and textural properties. In a previous work, the authors proposed the Multi-Layer Fusion-MRF (ML-FMRF) model (Szirányi and Shadaydeh 2014) for optical image segmentation and change detection. The superiority of the ML-FMRF model with comparison to other state-of-the-art supervised methods was already shown in (Benedek et al. 2015). The ML-FMRF model can be applied on the fusion of different image modalities (e.g. MS, ALS, etc.) from very different sampling time instants, or partially valid ground truth annotation actions. This solution is investigated in this paper for wetland classification using multitemporal MS data and a wetland classification map derived from ALS data from an earlier year.

While most techniques proposed in the literature are supervised methods requiring large amounts of training data, the proposed model can be used either as an unsupervised model on two MS images only, or as a semi-supervised model using ALS and MS data fusion. Here, the term 'semi-supervised' means that the ALS data is used for the initial training in one time iteration only (or whenever available); the classification model can then be applied on MS image time series while recursively integrating new MS images with the previous classification map without the further need for expensive ALS data or human interaction.

We present quantitative evaluation results of the model over the Lake Balaton test area, and validate it by using manually interpreted high resolution aerial imagery. The results of different types of data are compared, including standalone ALS and MS data and their fusion, justifying the superiority of fusing both data sources over using only a single data source.

2.   Materials and methods
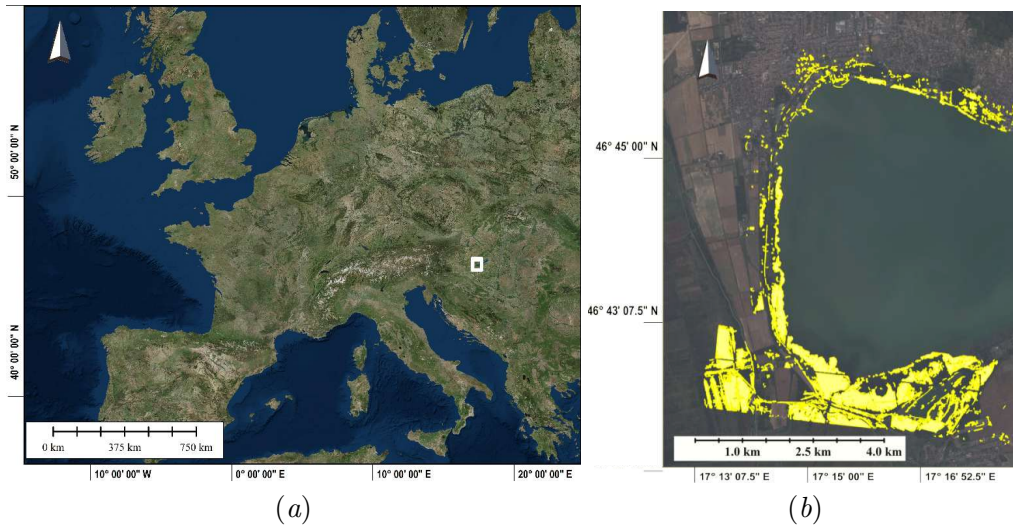
2.1.   *Study area*

Figure 1. (*a*) Study area in Europe, Hungary (OpenStreetMap), western part of Lake Balaton marked with the white rectangle; (*b*) Study area: wetland vegetation marked with yellow, based on the fieldwork in (Zlinszky et al. 2012).

The study area covers 80 km^2 around the town of Keszthely at the westernmost end of Lake Balaton (Figure 1). Despite its population of more than 20 000, Keszthely has a rather unique ecological setting as an urban center surrounded by an ecological matrix of relatively intact natural habitats. The small urban wetland patches along the shore promenade, harbours and beaches of Keszthely are crucial for sustaining the connectivity of one of the largest unbroken wetland systems in Hungary.

2.2.   *Applied data*

Two very high resolution multispectral Pleiades images were used for vegetation mapping along with the available 2010 ALS data (EUFAR AIMWETLAB survey). The attributes of the Pleiades images and the ALS data are summarized in Table 1.

The Pleiades satellites were launched in December 2011 (Pleiades 1A) and December 2012 (Pleiades 1B). The two satellites operate in the same phased orbit and they are offset at 180° with a mean altitude of 694 km. To get the best possible consistency between the Pleiades images and the 2010 ALS survey, we used two Pleiades image data acquired in August 2012 and June 2015. The chosen images, taken in August and June, represent two different agricultural seasons (post- and pre- harvest).

In addition to the two multispectral Pleiades images, we also use the available wetland vegetation classification map based on ALS data processing (Zlinszky et al. 2012). The ALS dataset was preprocessed by the NERC Data Analysis Node to the level of ASPRS ".las" files, and outlier points resulting from atmospheric or multi-path echoes were removed. Echo amplitudes were modulated by automatic gain control (AGC), and the AGC and amplitude values were included in the attributes of each point. After radiometric calibration and the identification of dropout points, an expert-generated decision rule-set was defined, with threshold values fine-tuned using a set

of 82 field-collected ground reference polygons (1010 m each) covering the full set of classes.

The full details of the study are explained in (Zlinszky et al. 2012) where "wetlands" were defined as areas where the soil is regularly fully saturated with water and where the vegetation is mainly composed of emergent macrophytes. The classification into 9 classes (6 wetland and 3 non-wetland) was done using an expert-generated decision tree with classification thresholds manually selected based on signature analysis. The ALS wetland classification map was generated by summing up the 6 wetland category class maps. For the 9 classes, (Zlinszky et al. 2012) reported a classification accuracy (Congalton 1991) of 82.71% and Cohen's Kappa (Jacob 1960) of 0.80. After merging the classes belonging to wetlands to a single category, they reported a user's accuracy of 100% and a producer's accuracy of 97%.

Table 1. Attributes of Pleiades MS satellite images and ALS data used in wetland mapping.

Sensor	Acquisition date	Attributes (unit)	Value
Pleiades	August 2012 June 2015	Spatial resolution (m): Spectral bands (μm):	2 Blue: $0.43 - 0.55$ Green: $0.50 - 0.62$ Red: $0.59 - 0.71$, NIR: $0.74 - 0.94$
Leica ALS50-II	August 2010	Wavelength(nm)	1064
		Pulse duration (ns)	4
		Scan angle (degree)	30
		Flying altitude (m)	1200
		Footprint size (cm)	22
		Mean ground point density (points m^{-2})	1
		Horizontal accuracy (m)	0.15
		Vertical accuracy (m)	0.10

2.3. *Proposed classification model*

MRF models are a useful solution for image segmentation, enabling multi-source fusion and hierarchical modeling. In a previous work (Szirányi and Shadaydeh 2014), the authors introduced a multi-layer MRF segmentation where multitemporal optical images of the same area were examined on different levels of the segmentation process. First, the combined features from multitemporal optical images were merged to form a multi-layer image. The goal was to enhance the definition of classes having high intraclass variations by using more sample layers while the small ratio of changed areas were considered as outliers and statistically excluded from the definition of classes of fused multiple layers. The MRF classification based label map of this multi-layer image was then used as training input for the classification of each separate optical image.

In this paper, the above Multi-Layer Fusion-MRF (ML-FMRF) model is further improved to fuse ALS data with multitemporal MS satellite imagery for the classification of wetlands.

The workflow of the improved ML-FMRF is illustrated in Figure 2. The proposed model consists of an unsupervised K-means clustering step followed by two MRF segmentation steps. It results in an unsupervised segmentation and change detection step at any later point in time using a preliminary ALS measurement as a reference.

In what follows, we first present a detailed description of the classification features,

followed by the main steps of the proposed ML-FMRF model.

2.3.1. Selection of classification features

An image $S = \{s_1, s_2, ...s_H\}$ is considered to be a two-dimensional grid of H pixels. We assume that K classes are present in the images and $\Lambda = \{\lambda_1, \ldots, \lambda_K\}$ is the set of all possible classes. Each of the image pixels may take a label λ from a finite set of labels Λ. Let $\Omega = \{\omega = (\omega_{s_1}, \ldots, \omega_{s_H}) : \omega_i \in \Lambda, 1 \leq i \leq H\}$ be the set of all possible labels assigned to the image pixels.

In a series of $N \geq 2$ registered images L_i, $i = 1, 2, \cdots, N$, for each pixel $s \in S$ in image L_i, we define the feature vector $\boldsymbol{x}_s^{L_i}$. This feature vector might contain a mixture of spectral, textural, and statistical values. For wetland classification in particular, we define $\boldsymbol{x}_s^{L_i}$ as:

$$\boldsymbol{x}_s^{L_i} = [R_s^{L_i}, G_s^{L_i}, B_s^{L_i}, (NIR)_s^{L_i}, (NDVI)_s^{L_i}]^T, \tag{1}$$

where $R_s^{L_i}$, $G_s^{L_i}$, $B_s^{L_i}$, and $(NIR)_s^{L_i}$ are respectively the Red, Green, Blue, and near infrared (NIR) channel values of this pixel; $(NDVI)_s^{L_i}$ is its NDVI value.

In addition to the spectral features of N multitemporal images, we also define a new statistical feature M_s which indicates the probability of pixel s being in a particular class $\lambda_c \in \Lambda$, i.e. $M_s = P(\omega_s = \lambda_c)$. The probability map $M^t = \{M_s, s \in S\}$ at an arbitrary time t is calculated from a classification map M^{t_0} acquired at a different time t_0 (before or after t) as follows:

$$M^t = \alpha M^{t_0} + \frac{(1-\alpha)}{\sigma} \mathcal{N}(0, \sigma). \tag{2}$$

That is, the probability map at a certain time t, can be calculated from a classification map at time t_0 with some uncertainty. This uncertainty is represented by white Gaussian noise $\mathcal{N}(0, \sigma)$ of zero mean and variance σ^2. In our study, we used the standard normal distribution $\mathcal{N}(0, 1)$. The variance σ^2 however could be defined based on the statistical analysis of measurement errors and the probability of change of this particular class if available. The parameter $\alpha \in]0, 1[$ is equal to the classification accuracy of the wetland class in M^{t_0}.

In this paper, we set the classification map M^{t_0} equal to the ALS wetland classification map described in Section 2.2. That is, we set $M^{t_0} = 1$ for pixels classified as wetland and $M^{t_0} = 0$ otherwise. The addition of the wetland class probability measure to the stack of features helps in removing the ambiguity from some of the class definitions. Hence, it improves the discrimination of land-cover classes with similar spectral characteristics such as agricultural areas and wetlands.

It should be noted that although ALS wetland classification results are used in this study to derive the wetland class probability map, any other classification results could have been used. It is possible for example to use classification results derived from MS data from previous years or different seasons, or to use other sensor classification data (e.g. SAR data classification).

2.3.2. Multi-Layer Fusion-Markov Random Field (ML-FMRF) model

The classification and change detection procedures, using the proposed ML-FMRF Model, are described in the following main steps (see Figure 2):
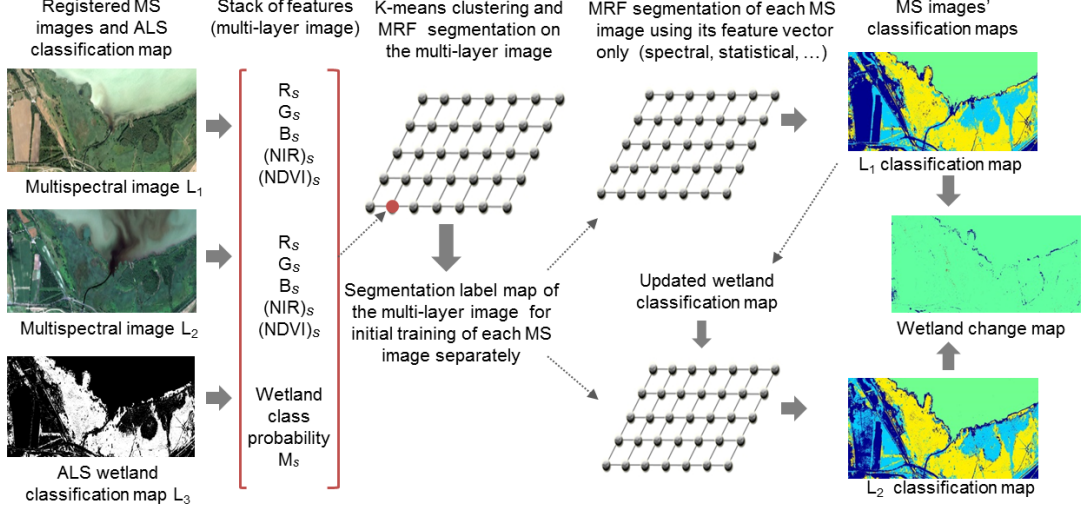
Figure 2. Workflow of the proposed Multi-Layer Fusion MRF (ML-FMRF) classification and change detection process.

(1) Registration of the MS images and the ALS wetland classification map.

(2) The feature vectors of the N multitemporal images in addition to the wetland class probability map are calculated using Equations 1 and 2 respectively, then combined to form the stack of feature vectors:

$$\boldsymbol{x}_s^{\text{fusion}} = \{\boldsymbol{x}_s^{\text{L}_1}, \boldsymbol{x}_s^{\text{L}_2}, ...\boldsymbol{x}_s^{\text{L}_N}, \text{M}_s\}. \tag{3}$$

(3) Finding clusters of the multi-layer image $\mathbf{X} = \{\boldsymbol{x}_s^{\text{fusion}}, s \in \text{S}\}$ and calculating cluster parameters (mean and variance) of the multi-layer image clusters. This step is performed using the unsupervised K-means algorithm. However, it is also possible to use supervised clustering algorithms if/when user interaction is needed.

(4) Running MRF segmentation on the multi-layer image $\mathbf{X}$ using the K-means clustering parameters to obtain the fusion labelling map Ω_{fusion} over the multi-layer image.

(5) The multi-layer labelling Ω_{fusion} is used as the training map for the classification of each MS image $\text{L}_i, i = 1, 2, \cdots, N$.

(6) For each MS image L_i, an MRF segmentation is performed on its spectral features $\boldsymbol{x}_s^{\text{L}_i}$, and possibly other textural and statistical features, resulting in a labelling Ω_{L_i}.

(7) The consecutive MS image layers $(..., (i-1), (i), ...)$ are compared to find the changes among the different label maps to get the $\delta_{i-1,i}$ change map:

$$\delta_{i-1,i}(s) = \left[\left(\Omega_{\text{L}_i}(s) \neq \Omega_{\text{L}_{i-1}}(s)\right) = \text{TRUE}\right]. \tag{4}$$

We use a Maximum A Posterior (MAP) estimator for the label field of the MRF in both stages (Steps 4 and 6). Here, we provide the details of the multi-layer MRF optimization (Step 4). We use a similar optimization for the single layer MRF as well (Step 6). In Step 4, the MAP estimator is realized by combining the conditional

random field of the observed data $P(\boldsymbol{x}_s^{\text{fusion}}|\omega_s)$ and the unconditional Potts model (Potts 1952). The global labelling $\widehat{\Omega}$ is defined by the energy minimum:

$$\widehat{\Omega} = \text{argmin}_\Omega \left[\sum_{s \in S} -\log P(\boldsymbol{x}_s^{\text{fusion}}|\omega_s) + \sum_{r,s \in S} \Theta(\omega_r, \omega_s) \right], \qquad (5)$$

where the minimum is searched over all the possible labellings (Ω) of the input, and the $\Theta(\omega_r, \omega_s)$ neighbourhood-energy term is zero if s and r are not neighbouring pixels, otherwise Θ can be modified by applying the β homogeneity weight:

$$\Theta(\omega_r, \omega_s) = \begin{cases} 0 & \text{if } \omega_r = \omega_s \\ +\beta & \text{if } \omega_r \neq \omega_s \end{cases} . \qquad (6)$$

The likelihood functions $P(\boldsymbol{x}_s^{\text{fusion}}|\omega_s)$ for all classes $\omega_s \in \Lambda$ are represented by the Gaussian distributions:

$$P(\boldsymbol{x}_s^{\text{fusion}}|\omega_s) = \frac{1}{(2\pi)^{d/2}|\boldsymbol{\Sigma}_{\omega_s}|^{1/2}} \exp\{-\frac{1}{2}(\boldsymbol{x}_s^{\text{fusion}} - \boldsymbol{\mu}_{\omega_s})^T \boldsymbol{\Sigma}_{\omega_s}^{-1}(\boldsymbol{x}_s^{\text{fusion}} - \boldsymbol{\mu}_{\omega_s})\}, \quad (7)$$

where d is the length of the feature vector $\boldsymbol{x}_s^{\text{fusion}}$. The mean and the covariance matrix of the K clusters (output of the K-means clustering in Step 3) are used for $\boldsymbol{\mu}_{\omega_s}$ and $\boldsymbol{\Sigma}_{\omega_s}$ respectively.

In our experiments, we set $\beta = 0.1$ and we used a graph cut based α-expansion algorithm (Szeliski et al. 2006) for the energy minimization of the MRF, with the implementation accompanying (Szeliski et al. 2006).

2.4. Validation method

The presented classification model is validated against independent aerial orthoimages (two sets of sub-meter resolution images). For the validation of the 2012 data, 40-cm resolution aerial orthoimages from August 2010 were used. These aerial images were collected in the same campaign as the ALS data (EUFAR AIMWETLAB survey). For validating the 2015 data, 30-cm resolution aerial orthoimages collected in March 2014 were used. Both image series were collected using a Leica RCD 105 camera (39 megapixels) in visible true colour RGB bands.

For sampling both the aerial orthoimages and the vegetation classification data, a regularly spaced grid of points was first generated at an even spacing of 100 m. Then these points were overlaid on the aerial imagery, and for each point the land cover class was registered based on the interpretation of an experienced operator, at scales between 1 : 1000 and 1 : 2000. This was done separately for the 2010 and the 2014 images.

The proposed model is applied on the test area using MS data alone as well as using MS/ALS data fusion. Confusion matrices are then calculated by comparing the classification results of both cases with the manual interpretation of aerial images.

It should be noted that the landscape may have changed between years 2010 and 2012. Here we had to balance between using high-quality independent reference data with a time lag (which was possible with the 2010 aerial images) or using lower quality, less independent but synchronous imagery (i.e. manual interpretation of the same 2012 Pleiades images). We wanted to be certain of the independence, accepting the fact that
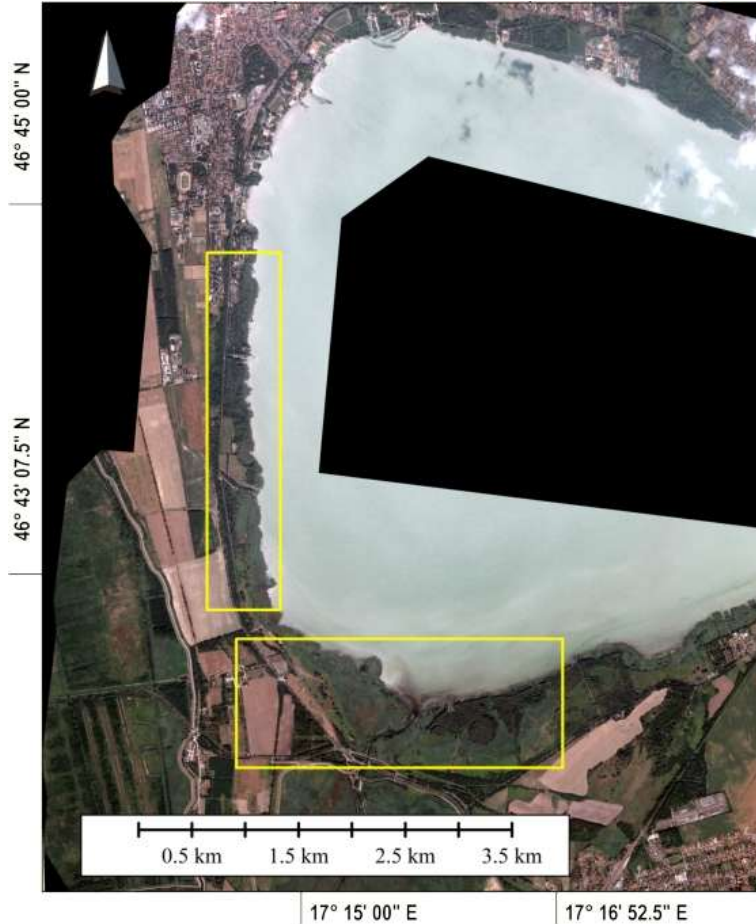
Figure 3. Pleiades satellite image of Keszthely, Lake Balaton with the two selected patches marked with yellow rectangle.

eventual changes in the landscape will decrease the accuracy. The accuracy figures we report in this paper include this error, thus we expect to obtain higher accuracy when using images with a smaller time difference.

3. Results and Discussion

3.1. *Wetland classification*

The fusion of multitemporal multi-sensor images involves several essential pre-processing steps including registration, re-sampling, and normalization. The multispectral and ALS datasets were all re-sampled to have the same spatial resolution of 2×2 m/pixel. Since for our experiments all images were provided as orthocorrected geo-referenced images, no further refined registration was required. The 80 km^2 (about 20 million pixels) test area is divided into patches of approximately 4 km^2 (about 1 million pixels) due to the computational constraints of the implemented MRF optimization method. Two representative patches (Figure 3) providing a challenging mixture of land cover classes are discussed in detail in this section. In our experiments we used the two available multispectral images of August 2012 and July 2015 (described in Section 2.2), which represent two different seasons, pre- and post-agricultural harvest.

However, it could be possible to use three or more images to further improve cluster definitions depending on the quality, seasons and lighting conditions of the images. The ideal season for the used MS images is after the agricultural harvest, when fields are already harvested, but before late September-early October when the wetland leaves start drying out. In addition to the two MS images, the wetland classification map based on the August 2010 ALS data (see Section 2.2) is used to generate the wetland class probability layer M^{t_0} in Equation 2 with classification accuracy $\alpha = 0.97$.

The main processing steps of the ML-FMRF classification in Section 2.3.2 are executed on the input layers: L_1 (August 2012 MS image shown in Figures 4-5 (a))), L_2 (August 2015 MS image shown in Figures 4-5 (b)), and L_3 (August 2010 wetland classification map based on ALS data shown in Figures 4-5 (d)). The unsupervised K-means clustering is applied with six classes on the fused multi-layer image using the *kmeans* function in MATLAB where a preliminary clustering phase on a random 10% subsample of the data is used to initialize cluster parameters.

Following the multi-layer fused classification, the single layer MRF classification of L_1 is performed using its spectral features only (R, G, B, NIR and NDVI values). In the single layer MRF classification of L_2, in addition to the spectral features, we use a new wetland class probability map derived from the classification map of L_1. The use of the wetland class probability map derived from the classification results of the August 2012 post-harvest image helps to improve the discrimination between wetland and agricultural fields in the pre-harvest image of June 2015.

To compare the classification accuracy using the fusion of ALS and MS data with those using MS data alone, experiments similar to the above were performed using only L_1 and L_2 as input layers. Classification results are shown in Figures 4-5 (e) and (f). Tables 2-6 show confusion matrices and classification accuracies for the 2012 and 2015 MS images, with and without ALS data fusion.

For the analysis of the obtained classification results, we have selected some specific regions marked with dashed lines in Figures 4-5 (a). Using single data source (ALS or MS only), we can observe that the agricultural area (marked with yellow dashed lines in Figure 4 (a) was misclassified as wetland when using only ALS data (Figure 4 (d)), but was classified successfully as 'Other land' using MS data alone. Similarly, the urban areas (marked with red dashed lines in Figure 5 (a)) were misclassified as wetland using ALS data alone, but correctly identified as urban areas using MS data. On the other hand, the two vegetation areas (marked with white dashed lines in Figure 5 (a)) were misclassified using only MS data, while they were correctly classified as wetlands using ALS data alone.

The quantitative analysis presented by the confusion matrices (Tables 2-5) shows that the confusion between 'Wetland' and 'Trees/Shrubs' classes is considerably reduced for both years when using MS and ALS fusion. The producer's accuracy of the wetland class is considerably improved from 81.37% to 84.57% for the year 2012 image and from 85.92% to 93.06% for the 2015 image. The overall accuracy is increased from 83.50% to 85.93% for the image of year 2012, and from 81.4% to 85.61% for the year 2015. This results in an increase in Cohen's Kappa from 0.78 to 0.81 for the 2012 image and from 0.75 to 0. 81 for the 2015 image.

However, the error in the ALS classification of the agricultural area (marked with yellow dashed lines in Figure 4 (a)), slightly decreased the accuracy of the fused classification results when comparing to the results using only MS data. For the August 2012 post-harvest image, this agricultural area shows as bare soil (Figure 4 (a)); the use of the spectral features of the MS images could correct the error in the ALS classification. However, for the June 2015 pre-harvest image, this agricultural area shows as

Table 2. Confusion matrix and user's accuracy of land cover classification of 2012 image using MS data only.

		Reference class			
		Water	Wetland	Trees/Shrubs	Other lands
	Water	153	1	1	3
Predicted	Wetland	0	131	16	14
class	Trees/Shrubs	0	28	80	8
	Other lands	1	9	8	86
	Total	154	169	105	111
	User's accuracy	99.3%	77.5%	76.2%	77.5%

Table 3. Confusion matrix and user's accuracy of land cover classification of 2012 image using MS/ALS data fusion.

		Reference class			
		Water	Wetland	Trees/Shrubs	Other lands
	Water	144	5	1	4
Predicted	Wetland	4	137	20	1
class	Trees/Shrubs	1	9	107	7
	Other lands	3	8	13	76
	Total	152	159	141	88
	User's accuracy	94.7 %	86.2%	76%	86.4%

Table 4. Confusion matrix and user's accuracy of land cover classification of 2015 image using MS data only.

		Reference class			
		Water	Wetland	Trees/Shrubs	Other lands
	Water	157	7	1	3
Predicted	Wetland	1	122	10	9
class	Trees/Shrubs	0	26	83	3
	Other lands	1	21	19	80
	Total	159	176	113	95
	User's accuracy	98.7%	69.3%	73.5%	84.2%

Table 5. Confusion matrix and user's accuracy of land cover classification of 2015 image using MS/ALS data fusion.

		Reference class			
		Water	Wetland	Trees/Shrubs	Other lands
	Water	155	5	4	0
Predicted	Wetland	1	134	8	1
class	Trees/Shrubs	1	4	105	5
	Other lands	1	22	27	76
	Total	158	165	144	82
	User's accuracy	98.1%	81.2%	72.9%	92.7%

green meadow (Figure 4 (*b*)) with spectral features close to the 'Trees/Shrubs' class; as a result, some parts of this agricultural area were misclassified as 'Trees/Shrubs'. The errors of the used wetland classification map (product of the 2010 ALS data) in the agricultural area as well as in the the marked urban areas as discussed above are the cause of the reduced producers accuracy of the 'Other land' class when using MS/ALS data fusion (Table 6).

It is important to note that the presented method is an unsupervised classification with only the wetland class having a prior definition, and the other classes receiving their labels after the classification. Thus, the expected classification accuracy of the non-wetland classes are less than they would be in case of pre-defined, supervised classification. In our study, the six classes are assigned the labels: water, wetland, trees, meadows, urban areas/shadow, and bare soil. Classification results are shown in Figures 4-5 (*g*) and (*h*). The three classes: meadows, urban areas/shadow, and bare soil are grouped in one class referred to as 'Other lands' and classification results are presented for 4 classes. The wetland ground truth based on field measurement

Table 6. Producers accuracy, overall accuracy, and Cohen's Kappa of classification results using MS data alone and using MS/ALS data fusion.

Dataset/Class	2012 MS	2012 MS + 2010 ALS	2015 MS	2015 MS + 2010 ALS
Water	96.8%	93.5%	93.5%	94.5%
Wetland	81.4%	84.6%	85.9%	93.1%
Trees/Shrubs	69.0%	86.3%	74.1%	91.3%
Other lands	82.7%	76.0%	66.1%	60.3%
Overall accuracy	83.5%	85.9%	81.4%	85.6%
Cohen's Kappa	0.78	0.81	0.75	0.81

performed in 2010 (Zlinszky et al. 2012) is added to Figures 4(*c*) and 5(*c*) for visual comparison.

3.2. *Multi-temporal change detection*

A major advantage of the ML-FMRF model is that the output of the multi-layer classification is used for the training of the single layers. As a result, similar classes are automatically given similar labels in all layers. Thus, based on the post-classification comparison, change maps can be directly generated by comparing the class labels of different layers. The change maps can provide the locations and the types of the changes simultaneously (see Section 2.3.2 and Equation 4). Figure 6 (*a*) and (*b*) show an example of detected changes in the wetland class between August 2012 and June 2015 using only multispectral data (Figure 6 (*a*)) and by fusion with ALS data (Figure 6 (*b*)). The detected changes are coloured according to their type as new wetland or deteriorated wetland. Visual comparison between images of 2012 and 2015 shown in Figure 4 (*a*) and (*b*) reflects similar changes. The validity and performance of the ML-FMRF model for change detection applications were compared with other state of the art methods in (Benedek et al. 2015) for optical images. However, the quantitative change analysis needs a temporal trajectory analysis of the related pixels which is out of the scope of the present paper; instead, we analyze the resulting data in a qualitative manner in the Discussion.

3.3. *Discussion*

The proposed unsupervised ML-FMRF model (without the use of the ALS reference map) delivered an overall classification accuracy comparable to that obtained by supervised models. For example, the overall accuracy of the ML-FMRF model using only two MS satellite images (8 spectral features) is comparable to the accuracy obtained by the supervised spatio-temporal contextual MRF approach (Wang et al. 2015) proposed for land cover mapping which reported an overall accuracy of 75.62%. The MRF approach in (Wang et al. 2015) uses eight Landsat 8 training samples and 144 features. The unsupervised K-means clustering followed by the multi-layer MRF in the proposed model provided an initial classification accuracy comparable to the supervised Random Forest classification used prior to MRF in (Wang et al. 2015). On the other hand, the combination of ALS with satellite imagery in the semi-supervised ML-FMRF model delivered accuracies comparable to the supervised decision tree classification approach proposed in (Rapinel, Hubert-Moy, and Clément 2015) where multi-sensor data (ALS, KOMPSAT-2 MS (4 ×4 m/pixel) and Quickbird MS (2.4 ×2.4 m/pixel)) were used for mapping different wetland types (hay meadow, reed beds, etc.) and reported a Kappa of 0.84. However, our results were obtained using only two MS images and
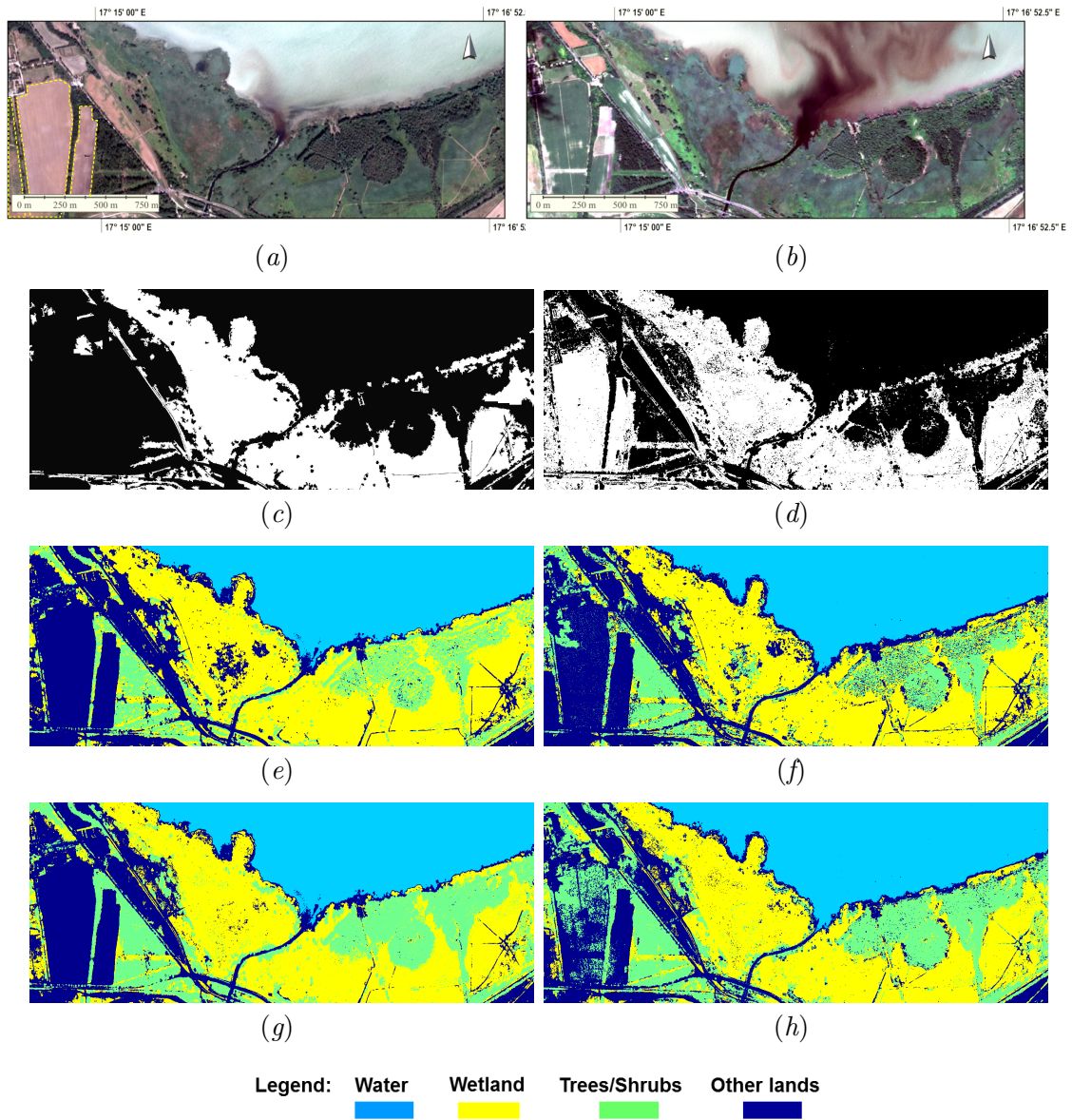
Figure 4. Land cover maps of Keszthely wetland (patch 1): (*a*) 2012 image (agricultural area samples are marked with yellow dashed lines), (*b*) 2015 image, (*c*) ground truth of wetland class (white) based on field measurement in 2010 (Zlinszky et al. 2012), (*d*) wetland classification map using 2010 ALS data (Zlinszky et al. 2012), (*e*) and (*f*) land cover classification maps using only MS data of years 2012 and 2015 respectively, (*g*) and (*h*) Land cover classification maps using MS and ALS data fusion for years 2012 and 2015 respectively.
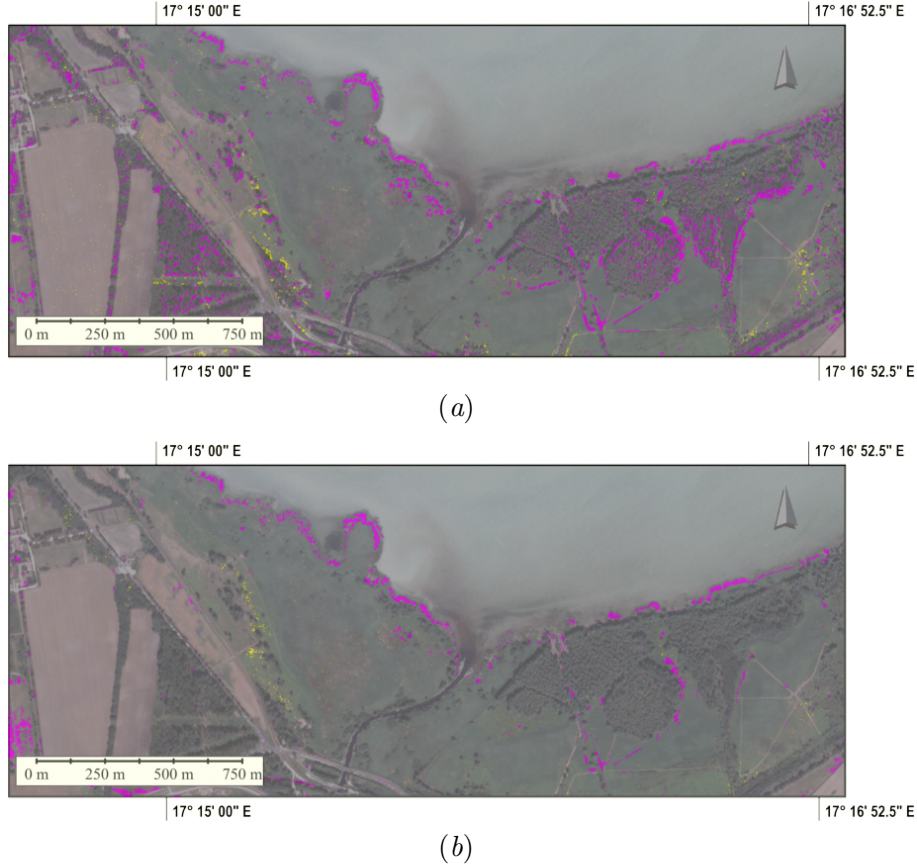
13

Figure 5. Land cover maps of Keszthely wetland (patch 2): (*a*) 2012 image (urban area samples are marked with red dashed lines; two vegetation area samples are marked with white dashed lines), (*b*) 2015 image, (*c*) ground truth of wetland class (white) based on field measurement in 2010 (Zlinszky et al. 2012), (*d*) wetland classification map using 2010 ALS data (Zlinszky et al. 2012), (*e*) and (*f*) land cover classification maps using only MS data of years 2012 and 2015 respectively, (*g*) and (*h*) land cover classification maps using MS and ALS data fusion for years 2012 and 2015 respectively.

14

Figure 6. Change map between years 2012 and 2015 using (*a*) MS data alone and (*b*) MS and ALS data fusion. New and deteriorated wetlands are shown in yellow and magenta colours respectively on 2012 image (patch 1).

ALS-based reference data acquired in a previous year and/or a different season, and the proposed method could achieve comparable accuracy in spite of changes in the land cover between the used MS images and the ALS data.

The ALS-MS fusion based classification results of the year 2012 post-harvest image can be used to derive the probability map for the classification of future MS images (this is already implemented in the classification of the year 2015 MS image). Hence, there is no further need to use ALS data again in future classifications. The proposed model can be used recursively for the automatic monitoring of land covers using remote sensing image time series. That is, the classification output of the proposed model at certain point in time can be used as a reference map for the classification of one or more new samples from a time series of MS images. Being a recursive solution, however, the performance of the proposed model depends on the accuracy of the initial conditions (ALS probability map in the proposed model), and/or the selection of the new samples (e.g. higher accuracy is observed for the after-harvest 2012 MS).

Since separating wetlands from non-wetland classes is the main objective of this study, only the wetland classification map is used. However, it is possible to add reference data for other categories in order to further improve the classification accuracy of the other classes. The choice of which classification results and which sensor data should be used to generate the probability map for a certain class is decided based on the classification accuracy of this certain class and/or its ability to incorporate

new information into the classification process. A possible future improvement could be to update the used reference map based on the integration of several previous classification maps or to use a probability map derived from fuzzy classification.

The main drawback of using MRF-based models for image segmentation/classification is its high computational complexity. In particular, an increase in the number of classes or the dimension of the classification feature vectors can negatively affect the performance of the classification. In our study we chose to apply the proposed classification methods to the main six land cover classes. Once the wetland class is detected, a similar ML-FMRF model can be applied to regions classified as wetlands to define different wetland vegetation subclasses. However, this approach needs further investigation. It is also worth to note that MS/ALS data fusion is performed neither on the decision level nor on the feature level, as it is the case for most data fusion methods proposed in the literature (see (Gomez-Chova et al. 2015) and references therein). Instead we generate one statistical feature derived from the wetland classification map of the ALS data to be fused with the spectral features of the MS data. We verified through exhaustive experiments that this type of fusion produces improved results and helps to eliminate the need for dimensionality reduction on the set of the ALS and MS data features.

4. Conclusions

This study demonstrates how high resolution ALS data and multitemporal multispectral satellite images can be fused to deliver high classification accuracy for regular monitoring of wetland extents and changes. The main steps of the presented approach are unsupervised K-means clustering followed by two stages of MRF segmentation. The fusion of multi-seasonal MS images (pre- and post-harvest images in this study) of the same area improved the discrimination between classes having high seasonal spectral variations, such as agricultural vegetation, trees, and wetlands. We use a wetland classification reference map derived from high resolution ALS data, improving the discrimination of land-cover classes with similar spectral characteristics. The ALS reference map is used for one time iteration only (or whenever available). The classification model can then recursively integrate new MS images with previous classification map. The experimental results of the developed classification model are validated against independent sub-meter resolution aerial images. Overall accuracies between 85 and 93 % for the wetland class and between 81 and 86 % for the 4 classes (Kappa 0.75-0.81) are observed over different years. We found that the fusion of ALS and MS data considerably improves the classification accuracy (3-6 percentage points in Kappa) compared to using only multispectral data. Our study sets the scene for the operational use of satellite data for regular high-resolution wetland monitoring, and allows the exploitation of the rich information contained in airborne data along with the high temporal resolution offered by satellite imagery. In the future, images obtained from recently deployed satellites could be used for fusion with ALS data from regional surveys.

References

Alonzo, Michael, Bodo Bookhagen, and Dar A. Roberts. 2014. "Urban tree species mapping using hyperspectral and lidar data fusion." *Remote Sensing of Environment* 148 (0): 70 83.

Benedek, Csaba, Maha Shadaydeh, Zoltan Kato, Tamás Szirányi, and Josiane Zerubia. 2015. "Multilayer Markov Random Field models for change detection in optical remote sensing images." *ISPRS Journal of Photogrammetry and Remote Sensing* 107: 22 – 37.

Berry, Pam, Alison Smith, Ric Eales, Liza Papadopoulou, Markus Erhard, Andrus Meiner, Annemarie Bastrup-Birk, et al. 2016. "Mapping and assessing the condition of Europe's ecosystems: progress and challenges –." *EEA contribution to the implementation of the EU Biodiversity Strategy to 2020* .

Congalton, Russell G. 1991. "A review of assessing the accuracy of classifications of remotely sensed data." *Remote Sensing of Environment* 37 (1): 35 – 46.

Davidson, Nick C. 2014. "How much wetland has the world lost? Long-term and recent trends in global wetland area." *Marine and Freshwater Research* 65: 934–941.

Eitel, Jan U.H., Bernhard Hfle, Lee A. Vierling, Antonio Abelln, Gregory P. Asner, Jeffrey S. Deems, Craig L. Glennie, et al. 2016. "Beyond 3-D: The new spectrum of lidar applications for earth and ecological sciences." *Remote Sensing of Environment* 186: 372 – 392.

Gomez-Chova, L., D. Tuia, G. Moser, and G. Camps-Valls. 2015. "Multimodal classification of remote sensing images: a review and future directions." *Proceedings of the IEEE* 103 (9): 1560–1584.

Jacob, Cohen. 1960. "A Coefficient of Agreement for Nominal Scales." *Educational and Psychological Measurement April 1960 20: 37-46, doi:10.1177/001316446002000104* 20: 37–46.

Kovács, M., G. Turcsányi, Z. Tuba, S.E. Wolcsánszky, T. Vásárhelyi, Á. Dely-Draskovics, S. Tóth, et al. 1989. "The decay of reed in Hungarian lakes." *Conservation and Management of Lakes, Akadémiai Kiadó, Budapest* 461–470.

Levick, Shaun R, Dominik Hessenmöller, and E-Detlef Schulze. 2016. "Scaling wood volume estimates from inventory plots to landscapes with airborne LiDAR in temperate deciduous forest." *Carbon Balance and Management* 11 (1): 1.

Lu, D., and Q. Weng. 2007. "A survey of image classification methods and techniques for improving classification performance." *International Journal of Remote Sensing* 28 (5): 823–870. http://dx.doi.org/10.1080/01431160600746456.

Mandanici, Emanuele, and Gabriele Bitelli. 2015. "Multi-Image and Multi-Sensor Change Detection for Long-Term Monitoring of Arid Environments With Landsat Series." *Remote Sensing* 7 (10): 14019.

Mui, Amy, Yuhong He, and Qihao Weng. 2015. "An object-based approach to delineate wetlands across landscapes of varied disturbance with high spatial resolution satellite imagery." *ISPRS Journal of Photogrammetry and Remote Sensing* 109: 30 – 46.

Niculescu, S., C. Lardeux, I. Grigoras, J. Hanganu, and L. David. 2016. "Synergy Between LiDAR, RADARSAT-2, and Spot-5 Images for the Detection and Mapping of Wetland Vegetation in the Danube Delta." *IEEE Journal of Selected Topics in Applied Earth Observations and Remote Sensing* PP (99): 1–16.

Pfeifer, Norbert, Gottfried Mandlburger, Philipp Glira, Andreas Roncat, Werner Mücke, and András Zlinszky. 2015. "Lidar: Exploiting the Versatility of a Measurement Principle in Photogrammetry." In *Photogrammetric Week 2015, Stuttgart, Germany.*, 105 – 118. Wich-

mann.

Potts, R. 1952. "Some generalized order-disorder transformation." In *Proceedings of the Cambridge Philosophical Society*, 106.

Rapinel, Sébastien, Laurence Hubert-Moy, and Bernard Clément. 2015. "Combined use of LiDAR data and multispectral earth observation imagery for wetland habitat mapping." *International Journal of Applied Earth Observation and Geoinformation* 37: 56 – 64.

Reis, Vanessa, Virgilio Hermoso, Stephen K. Hamilton, Douglas Ward, Etienne Fluet-Chouinard, Bernhard Lehner, and Simon Linke. 2017. "A Global Assessment of Inland Wetland Conservation Status." *BioScience* 67 (6): 523. + http://dx.doi.org/10.1093/biosci/bix045.

Szeliski, R., R. Zabih, D. Scharstein, O. Veksler, V. Kolmogorov, A. Agarwala, M. Tappen, and C. Rother. 2006. "A Comparative Study of Energy Minimization Methods for Markov Random Fields." In *European Conference on Computer Vision*, Vol. 2, Graz, Austria, 16–29.

Szirányi, Tamas, and Maha Shadaydeh. 2014. "Segmentation of Remote Sensing Images Using Similarity-Measure-Based Fusion-MRF Model." *IEEE Geosci. Remote Sens. Lett.* 11 (9): 1544–1548.

Vymazal, Jan. 2011. "Enhancing ecosystem services on the landscape with created, constructed and restored wetlands." *Ecological Engineering* 37 (1): 1 – 5.

Wang, Jie, Congcong Li, Luanyun Hu, Yuanyuan Zhao, Huabing Huang, and Peng Gong. 2015. "Seasonal Land Cover Dynamics in Beijing Derived from Landsat 8 Data Using a Spatio-Temporal Contextual Approach." *Remote Sensing* 7 (1): 865.

Weier, John, and David Herring. 1999. "Measuring Vegetation (NDVI & EVI)." *Earth. Observatory, NASA, USA.* .

Whiteside, Timothy G., and Rene E. Bartolo. 2015. "Mapping Aquatic Vegetation in a Tropical Wetland Using High Spatial Resolution Multispectral Satellite Imagery." *Remote Sensing* 7 (9): 11664.

Zlinszky, A., W. Mücke, H. Lehner, C. Briese, and N. Pfeifer. 2012. "Categorizing wetland vegetation by airborne laser scanning on Lake Balaton and Kis-Balaton, Hungary." *Remote Sensing* 4 (6): 1617–1650.

Zlinszky, A., V. Toth, P. Pomogyi, and G. Timar. 2011. "Initial report of the Aimwetlab Project: simultaneous airborne hyperspectral, lidar and photogrammetric survey of the full shoreline of Lake Balaton, Hungary." *Geographia Technica* 11: 101–117.

Zlinszky, András. 2013. "Mapping and assessing the condition of Europe's ecosystems: progress and challenges." *PhD thesis Etvs Lornd University Budapest, 2013* .